CARBON 49 (2011) 4050–4058

available at www.sciencedirect.com

ScienceDirect

journal homepage: www.elsevier.com/locate/carbon

Single Pd atoms in activated carbon fibers and their contribution to hydrogen storage ☆

Cristian I. Contescu [a,*], Klaus van Benthem [b], Sa Li [c], Cecile S. Bonifacio [b], Stephen J. Pennycook [a], Puru Jena [c], Nidia C. Gallego [a]

[a] Oak Ridge National Laboratory, Materials Science and Technology Division, 1 Bethel Valley Road, Oak Ridge, TN 37831, USA
[b] University of California at Davis, Department of Chemical Engineering and Materials Science, 1 Shields Ave., Davis, CA 95616, USA
[c] Commonwealth University of Virginia, Department of Physics, Richmond, VA 23284, USA

ARTICLE INFO

Article history:
Received 20 December 2010
Accepted 14 May 2011
Available online 20 May 2011

ABSTRACT

Palladium-modified activated carbon fibers (Pd-ACF) were synthesized by melt-spinning, carbonization and activation of an isotropic pitch carbon precursor premixed with an organometallic Pd compound. The hydrogen uptake at 25 °C and 20 bar on Pd-ACF exceeded the expected capacity based solely on Pd hydride formation and hydrogen physisorption on the microporous carbon support. Aberration-corrected scanning transmission electron microscopy (STEM) with sub-Ångstrom spatial resolution provided unambiguous identification of isolated Pd atoms occurring in the carbon matrix that coexist with larger Pd particles. First principles calculations revealed that each single Pd atom can form Kubas-type complexes by binding up to three H_2 molecules in the pressure range of adsorption measurements. Based on Pd atom concentration determined from STEM images, the contribution of various mechanisms to the excess hydrogen uptake measured experimentally was evaluated. With consideration of Kubas binding as a viable mechanism (along with hydride formation and physisorption to carbon support) the role of hydrogen spillover in this system may be smaller than previously thought.

© 2011 Elsevier Ltd. All rights reserved.

1. Introduction

The use of high surface area carbon materials for hydrogen storage continues to attract interest because of the significant advantage of carbon being light-weight and reasonably inexpensive. However, physisorption of H_2 on nanoporous carbon, although significant at cryogenic temperatures, is too weak (with binding energies between 0.05 and 0.10 eV) and does not allow significant storage levels at near-ambient temperatures [1]. A possible method for increasing the interaction strength was suggested by quantum mechanical calculations. The mechanism (known as Kubas-type binding) is based on molecular polarization and multiple σ-bonding of H_2 molecules with *d* orbitals of transition metal atoms [2] or ions [3]. It was predicted that decoration of carbon materials with single atoms of alkali, alkaline–earth [4–6] or transition metals (TM) [7–9] would increase adsorption energy to the desired range of 0.25–0.60 eV, as needed for reversible operation at near-ambient temperatures and moderate pressures. However, while theoretical studies predicted high potential for hydrogen storage on metal-decorated carbon supports, the experimental verification was beset by difficulties. To the best

☆ *Notice:* This submission was sponsored by a contractor of the United States Government under Contract DE-AC05-00OR22725 with the United States Department of Energy. The United States Government retains, and the publisher, by accepting this submission for publication acknowledges that the United States Government retains, a nonexclusive, paid-up, irrevocable, worldwide license to publish or reproduce the published form of this submission, or allow others to do so, for United States Government purposes.

* *Corresponding author:* Fax: +1 865 576 8424.
E-mail address: ContescuCI@ornl.gov (C.I. Contescu).

0008-6223/$ - see front matter © 2011 Elsevier Ltd. All rights reserved.
doi:10.1016/j.carbon.2011.05.021

of our knowledge, the only experimental evidence of Kubas-type complexes for hydrogen storage was reported for organometallic Ti complexes [10] and mesoporous Ti oxides [11]. Most transition metals tend to cluster or aggregate into nanoparticles rather than remain as isolated atoms. Clustering lowers the capacity for hydrogen storage and drastically changes the mechanism: from Kubas binding to single atoms to chemisorptive dissociation on large particles and, for some TM, hydride formation [12]. In particular, clustering is both energetically favorable and kinetically possible for TM atoms supported on carbon nanostructures (fullerenes, nanotubes) because carbon–metal interactions are weaker than bulk cohesive energy and kinetic barriers opposing surface diffusion are absent [13,14].

Palladium is a particular case because of its capacity to form an interstitial hydride (β-$PdH_{0.67}$) that saturates quickly at room temperature and low H_2 pressures. This phase was identified as the active phase of Pd-based hydrogenation catalysts. With lowering the size of Pd nanoparticles, the H/Pd ratio in β-hydride diminishes from the bulk value (0.67) [15], but the pressure range of phase transformation at room temperature does not change [16]. Several groups reported that Pd-containing carbon materials have higher H_2 capacity at near-ambient temperatures than their Pd-free analogs, in spite of an apparent blockage of porosity available for physisorption [16–23]. According to numerous reports, the net increase in hydrogen uptake exceeds the amount consumed with hydride formation at the temperature and pressure conditions of the experiment. The difference was attributed to a cooperative effect between palladium particles and the carbon support [16,17] initiated by hydrogen spillover [18–23]. The latter is a well known mechanism of catalytic hydrogenation and involves H_2 dissociation on Pd and migration of H atoms to remote sites on the support. Indirect proof for H spillover in Pd–carbon materials came from neutron scattering measurements which showed formation of new C–H bonds after exposure to hydrogen at near-room temperature [24]. On the other hand, simulations have shown that migration of H atoms from Pd_4 clusters to a carbon support is favorable with some restrictive conditions [25,26], whereas single Pd atoms on graphenes and carbon nanotubes can bind at least two H_2 molecules per Pd site in Kubas complexes [27]. Therefore, if single Pd atoms could be stabilized on high surface area carbons, they may contribute multiple σ-bonding per metal atom with binding energies higher than physisorption, which would enhance the capacity of carbon near room temperatures and at moderate pressures.

In this paper we report successful synthesis of Pd-modified activated carbon fibers (Pd-ACF) with a large fraction of Pd as isolated single atoms. Positive identification of single Pd atoms and microstructural details of the carbon matrix support were obtained from atomic resolution aberration-corrected scanning transmission electron microscopy (STEM). Based on theoretical study of σ-bonding of H_2 to single Pd atoms on graphene, we attempt a first quantitative assessment of the contribution of various competing mechanisms for hydrogen storage in Pd-ACF. Addition of Pd causes an increase of about 25–30% of the hydrogen capacity compared to Pd-free activated carbon (at 25 °C and 20 bar). While a combination of Kubas-binding and hydride formation may explain this result in part, they cannot account quantitatively for all excess uptake measured experimentally. This leaves room for H spillover but in lower proportion than previously believed. A major fraction of adsorbed hydrogen is physisorbed on the carbon support.

2. Experimental details and computational techniques

2.1. *Materials synthesis and hydrogen uptake*

Pd-containing and Pd-free ACF were synthesized at Clemson University from isotropic petroleum pitch using the same general procedure described previously [28,29]. The carbon source was the same isotropic petroleum pitch procured from Chungnam National University, Daejon, Korea which was used in a previous work [29]; however this material is different from the gas-extracted fraction of an domestic pitch used in another publication [24]. An organometallic compound, palladium (II) acetylacetonate, was homogeneously mixed with pitch at a temperature just below the pitch softening temperature (230 °C). After melt-spinning at 250 °C the fibers were stabilized by slow oxidation in air (165–265 °C), and then heat-treated at 840 °C under a flow of CO_2 for simultaneous carbonization and physical activation. This treatment, which shortens the exposure time to high temperatures, was found [28,30] to produce Pd-ACF materials with smaller average size of metal particles, and at the same time, to maximize BET surface area and porosity of resulting materials, compared with those obtained through separate steps of carbonization in N_2 followed by physical activation in CO_2 [29]. The estimated burn-off (relative to the calculated weight after carbonization) was 40% for ACF and 45% for Pd-ACF. Physical parameters measured with N_2 adsorption at 77 K and CO_2 adsorption at 273 K are similar for both samples (Table 1), which allowed us to assume that the physisorption properties of the carbon support did not change after addition of Pd. More details about the synthesis process and the quantitative calculations based on it are provided in the Supplementary information file available on-line.

Hydrogen sorption isotherms were measured at 25 °C by the microgravimetric method using IGA 01 from Hiden Isochema. A typical example is plotted in Fig. 1 for pure ACF and Pd-modified ACF. The samples (~80–90 mg) were outgased *in situ* at 300 °C for 12 h prior to measurements. Research grade H_2 (99.9999%) was used, which was passed through a liquid N_2 trap to retain condensable impurities. Gas compressibility corrections were made using the Peng–Robinson equation of state. Buoyancy corrections were made based on helium density measurements (Quantachrome ultrapycnometer) for ACF (1.77 g/cm^3) and Pd-ACF (1.86 g/cm^3) before activation, adjusted correspondingly for the actual Pd weight fraction (2.55%) in the activated sample with 45% burn-off. See Supplementary information file for details. A value of 0.01 g/cm^3 was assumed for the density of adsorbed hydrogen, which was obtained by comparing the maximum H_2 uptake measured gravimetrically with the micropore volume, and represents 15% of the density of liquid hydrogen (0.071 g/cm^3). In our experimental conditions (low uptake,

Table 1 – Physical properties of Pd-free and Pd-modified activated carbon fibers.

	Surface area[a] (m^2/g)	Total pore volume[b] (cm^3/g)	Micropore volume[c] (cm^3/g)	Ultramicropore volume[d] (cm^3/g)
ACF	1996	0.86	0.80	0.32
Pd-ACF	1990	0.91	0.83	0.29

[a] BET method.
[b] N_2 adsorption at $p/p_o = 0.995$.
[c] $d < 2$ nm from N_2 adsorption at 77 K, DFT-NL method.
[d] $d < 0.7$ nm from CO_2 adsorption at 273 K, DFT-NL method.

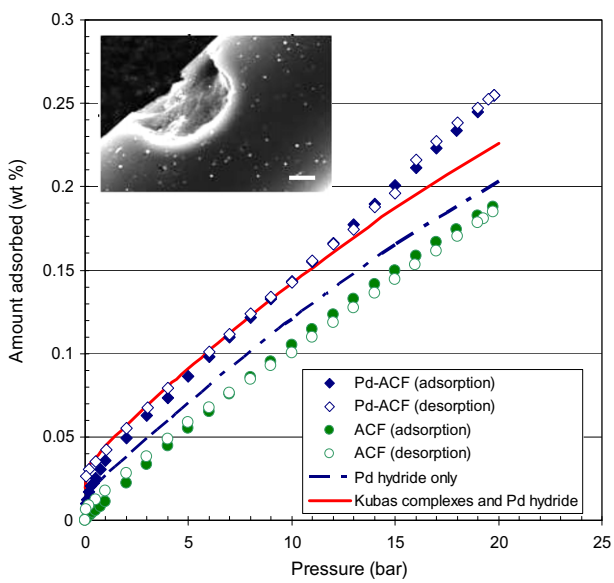

Fig. 1 – Hydrogen isotherms measured at 25 °C for ACF (circles) and Pd-ACF (solid diamonds, adsorption; open diamonds, desorption) and the amounts expected for Pd-ACF if (1) all Pd is converted to $PdH_{0.67}$ (dot-dashed line) and (2) atomic Pd forms Kubas complexes with pressure-dependent stoichiometry, and Pd nanoparticles convert to Pd hydride (red line, see text for details). The inset shows a scanning electron microscope image of Pd-ACF, demonstrating that Pd particles (bright intensities) are homogeneously distributed throughout the volume of carbon fibers. (For interpretation of the references to color in this figure legend, the reader is referred to the web version of this article.)

moderate pressure, room temperature) the total adsorption is practically indistinguishably close to the true surface excess adsorption as defined by Gibbs. The accuracy of IGA measurements was estimated at ±0.01 wt.% for the conditions used in these tests (100 mg sample, maximum pressure 20 bar, room temperature). The approach to equilibrium after each incremental increase in hydrogen pressure was dynamically monitored in real time by the IGA software. The equilibration was fast, and the weight approached asymptotically a stable value in less than 15 min. Examples of kinetic curves for H_2 adsorption on Pd-ACF are provided in the Supplementary information file. The weight readings were verified through quantitative measurement of Pd hydride formation from Pd nanopowder.

2.2. *Structural characterization*

For STEM investigations, fibers were ground in a methanol slurry and drop deposited onto holey carbon film mounted on TEM specimen grids. Annular dark-field (ADF) STEM images, often referred to as Z-contrast images, are sensitive to heavy elements since the scattering cross-section is roughly proportional to the squared atomic number Z^2 of the illuminated species [31]. Bright-field (BF) STEM images are sensitive to lighter elements, so that simultaneous acquisition of ADF and BF signals with pixel-to-pixel correlation is efficient for the investigation of carbon microstructures in the presence of catalytic Pd particles. Experiments were carried out using the aberration-corrected HB 603 U dedicated STEM that is operated at 300 keV and provides electron probe sizes below 1 Å [32]. In addition, energy dispersive X-ray spectroscopy was carried out with a Hitachi HD-2000 STEM to confirm that impurity concentrations were insignificant in the investigated samples.

2.3. *Simulations of $Pd(H_2)_n$ @ graphene structure*

The so-called Kubas interaction between dihydrogen and supported TM atoms or positively charged metal ions involves forward charge donation of the σ bonding electrons in H_2 to partially filled *d* orbitals of TM atoms and back-donation from the metal atom to the σ^* anti-bonding orbital of H_2 [2]. In addition, metal cations can bind hydrogen quasi-molecularly by a charge polarization mechanism [3]. First principles calculation was used to answer the question on how many hydrogen molecules can a Pd atom bind when supported on graphene. After determining the preferred site of a Pd atom on graphene and the corresponding binding energy, hydrogen molecules were gradually introduced until no variations in distance between Pd and graphene was recorded before and after hydrogen loading.

The relaxation and electronic structure were calculated using Vienna *ab initio* simulation package (VASP) [33] and the projector augmented wave (PAW) [34] method. The PAW GGA [35] potentials with the valence states 4*d* and 5*s* for Pd, and 2*s* and 2*p* for C were used. High precision calculations with a cutoff energy of 500 eV for the plane-wave basis were performed. The atomic coordinates were optimized with the shape and volume of the supercell fixed. For sampling the irreducible wedge of the Brillouin zone we used *k*-point grids of $1 \times 1 \times 1$ for the graphene calculations. In all calculations, self-consistency was achieved with a tolerance in the total energy of at least 0.1 meV. Spin-polarized calculations were carried out, and Pd-doped carbon is found to be nonmagnetic.

3. Results and discussion

3.1. Structural analysis

ADF STEM imaging of Pd-ACF revealed a median Pd particles diameter of (9.66 ± 1.50) nm throughout the volume of the fibers with roughly 66% of the metal particles smaller than 5 nm. Fig. 2 shows a pair of simultaneously acquired ADF and BF images. The ADF image (Fig. 2a) shows a Pd nanoparticle with a size of roughly 5 nm, while the BF image (Fig. 2b) reveals lattice fringes for the Pd-ACF. In some areas, the carbon microstructure exhibits local short-range ordering with up to five quasi-parallel graphene sheets, while in other areas image contrasts indicate disordered or even amorphous carbon.

In areas where the projected specimen thickness is sufficiently small, ADF STEM images revealed highly localized areas with bright intensities and diameters below 1 Å (see Fig. 3a). The simultaneously acquired BF-STEM images (Fig. 3b) are not sensitive to single Pd atoms, but offer detailed information about the carbon microstructure that supports the isolated catalyst atoms. A quantitative analysis of image intensities combined with through-focal series image acquisition [36–40] unambiguously identified such image intensities to represent single Pd atoms dispersed in the microporous carbon structure (see following paper [41] in this issue). The potential formation of dimers, trimers, etc. was not observed. Analysis of many different areas on multiple STEM samples [41] showed that single Pd atoms are positioned in several reoccurring structural arrangements identified in the carbon microstructure. Most frequently identified structures comprise open volumes between diverging graphene sheets, positions surrounded by multiple graphene layers with almost concentric arrangement, or locations in rather amorphous carbon zones with no graphitic fringes visible at short distance. More details and images of these reoccurring structures are presented in a separate letter [41].

The presence of single Pd atoms is related to the particular synthesis route chosen for Pd-ACF [29]. Rather than depositing the metal on preformed carbon substrates, as other groups have done [16–19], we added the Pd acetylacetonate complex, $Pd(acac)_2$, to the carbonaceous pitch precursor *before* melt-spinning and carbonization. This has important consequences because the Pd^{2+} ions formed through thermal decomposition of the organometallic precursor interact with the polyaromatic hydrocarbons in pitch and modify the resulting microstructure in carbon [42]. Recently published first-principles simulation [43] revealed the chain of chemical transformations during thermal processing (at 500 °C) of Pd $(acac)_2$ mixture with a polyaromatic hydrocarbon, chrysene, one of the main components of the isotropic pitch variety used in this study [44]. The results show that after decomposition of the $Pd(acac)_2$ complex, one acetylacetonate fragment cross-links to a chrysene molecule, while Pd is first associated with the second acac ligand and eventually develops σ bonding to another chrysene molecule. As a result, some fraction of palladium is maintained in atomic dispersion state, as shown by our microscopy results. The work cited [43] validates our working hypothesis on the development of strong interactions between Pd^{2+} and the carbon precursor prior to carbonization [29,42]. The observation of single Pd atoms represents indirect evidence for strong interactions of single atoms with the support, similar with observations reported for other catalytic systems [38–40,45–47]. However, clustering and aggregation could not be avoided during thermal processes (carbonization, activation) and a large fraction of palladium forms nanometer-size particles which reduce to metal even before exposure to hydrogen [48].

3.2. Simulations of σ-bonded H_2 to single Pd atoms on graphene

The objective of our calculations was to determine the stoichiometry, binding energies, and the structure of Kubas-type complexes formed from binding of multiple H_2 molecules to single Pd atoms on graphene. Calculations were carried out in two steps: (1) H_2 interactions with a bare Pd atom, and (2) H_2 interaction with a Pd atom supported on graphene.

When hydrogen molecules are interacted with a bare Pd atom, they all bind in molecular form, although the H–H

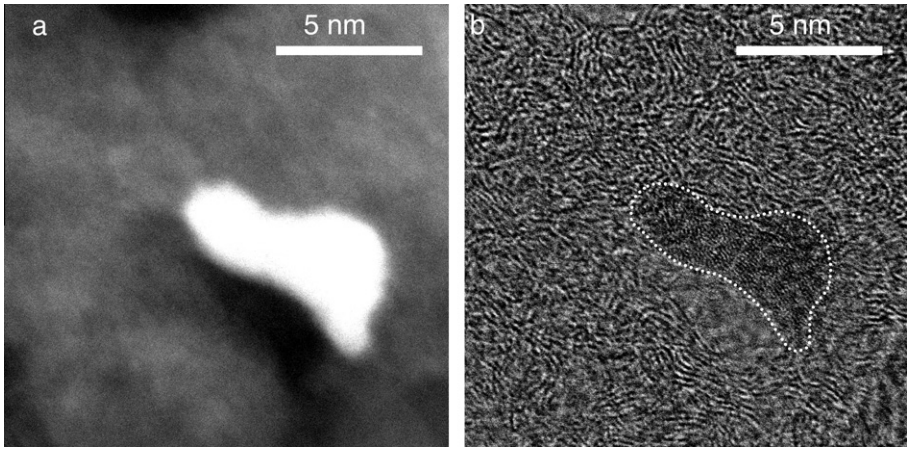

Fig. 2 – Pair of simultaneously acquired ADF (a) and BF (b) STEM images. The bright image contrasts in (a) represent a Pd nanoparticle. The BF image (b) is sensitive to the carbon microstructure and shows several domains with quasi-parallel graphene layers. The dotted line in (b) marks the location of the Pd nanoparticles.

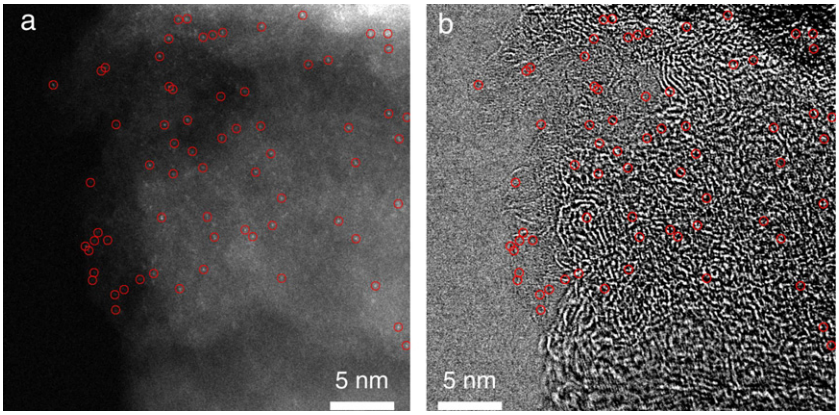

Fig. 3 – Pair of ADF (a) and BF (b) STEM images to correlate the location of single Pd atoms (encircled) with the supporting carbon microstructure. In (b), carbon atoms are represented by bright fringes due to a positive defocus parameter.

bonds are stretched from their normal value of 0.76 Å (Fig. 4). The extent of stretching depends upon the number of H_2 molecules (n) attached. The first H_2 molecule is stretched the most. As n increases, the H–H distance diminishes and the Pd–H bond length increases. These changes are reflected in the binding energies of H_2 which decrease as n increases. The average binding energies are given in Table 2. Three H_2 molecules bind to the Pd atom in a planar structure with Pd–H distance of 1.77 Å and H–H distance of 0.85 Å. A Pd atom can bind maximum $3H_2$ molecules with average binding energy of 0.86 eV/H_2. Further addition of H_2 leads to a metastable state where H_2 is at a distance of 2.40 Å from the Pd atom and the H–H distance is 0.76 Å.

Next we studied hydrogen interaction with a Pd atom supported on graphene. To study the preferred site of Pd on graphene we started by placing the Pd atom on various sites. We considered three sites: on top of the hexagonal hollow site, above the carbon site, and above the C–C bridge site. Binding energies were calculated for each of these configurations. The Pd atom moved to the top of the bridge site irrespective of the starting configuration. The resulting binding energy of Pd to graphene, namely 1.04 eV, is smaller than H_2 binding energy of 1.11 eV to a bare Pd atom. This shows that Pd would prefer to bind to H_2 rather than to graphene. The

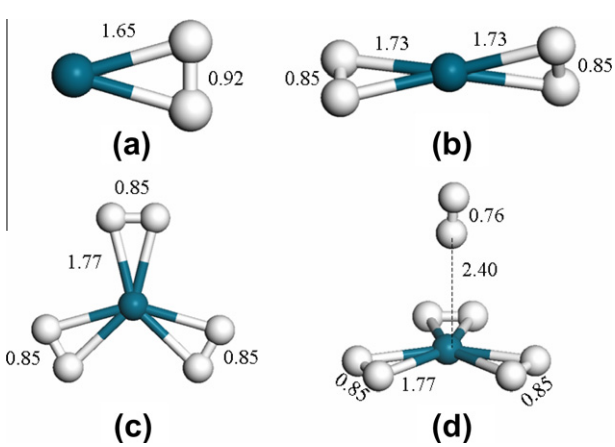

Fig. 4 – Geometry of (a) PdH_2 (C_{2v} point group), (b) $Pd(H_2)_2$ (D_{2d} point group), (c) $Pd(H_2)_3$ (D_{3h} pint group) and (d) $Pd(H_2)_4$ (C_1 point group).

preferred C–C bridge site of Pd is in agreement with recent calculation [49]. The distance between Pd and the nearest C atom is 2.20 Å.

Next, the influence of Pd atoms on hydrogen uptake was studied by adding H_2 molecules to each Pd atom successively and optimizing the corresponding geometry (Fig. 5). The first H_2 is bonded to Pd atom in a quasi-molecular form with H–H distance of 0.86 Å and Pd–H distance of 1.72 Å. The Pd atom is 2.18 Å away from the nearest C atom on the graphene surface. Since Pd atom is bonded both to graphene and H_2, the binding between Pd and H_2 molecule is reduced to 0.96 eV from 1.11 eV corresponding to bonding of H_2 to a free Pd atom. With the addition of the second H_2 molecule, Pd moves slightly away from graphene surface, namely at 2.49 Å, with Pd–H distance of 1.75 Å and H–H distance of 0.85 Å. Upon the addition of the third molecule, the $Pd(H_2)_3$ complex continues to move away from the graphene surface to a Pd–C distance of 3.68 Å. The three hydrogen molecules bind to the Pd atom at an average Pd–H distance of 1.77 Å. The H–H distance remains nearly the same at 0.85 Å. After the fourth H_2 molecule is added the resulting $Pd(H_2)_4$ cluster moves even further away from the graphene surface. The distance between Pd and nearest carbon on the surface is 3.8 Å. The fourth H_2 molecule is at a distance of 2.39 Å from the Pd atom and the H–H distance reduces to 0.76 Å. To explain why the $Pd(H_2)_n$ complex moves away from graphene when three of more H_2 molecules are attached, we compare in Table 2 the following energies: (1) the binding energy of a free Pd bound to nH_2, $(\Delta E^{Pd})_n = Pd(H_2)_n - Pd - nH_2$ and (2) the binding energy of Pd bound to both nH_2 and graphene, $(\Delta E^{PdC})_n = Pd(H_2)_n$ @ graphene – Pd – graphene – nH_2. Table 2 shows that the affinity of $Pd(H_2)_n$ binding to graphene decreases with increasing n. $Pd(H_2)_n$ (n = 1 and 2) prefer to bind to graphene surface, since ΔE^{PdC} is higher than ΔE^{Pd}. But starting from the third H_2 molecule, ΔE^{PdC} is almost equal to ΔE^{Pd}, which suggests that the interaction between $Pd(H_2)_n$ (n = 3 and 4) and graphene is negligible. The above energies together with the average binding energies of H_2 to bare and graphene-stabilized Pd atoms, E^{Pd} and E^{PdC}, are given in Table 2. The latter were defined as follows:

$$E_n^{Pd} = \frac{Pd(H_2)_n - Pd - nH_2}{n}$$

Table 2 – ΔE^{Pd}, ΔE^{PdC}, average binding energies for H_2 in $Pd(H_2)_n$ and $Pd(H_2)_n$ @ graphene Kubas-type complexes, and estimated equilibrium pressures for formation of $Pd(H_2)_n$ @ graphene at 300 K.

n	ΔE^{Pd} (eV)	ΔE^{PdC} (eV)	E^{Pd} (eV)	E^{PdC} (eV)	P (bar)
1	1.11	1.99	1.11	0.96	6×10^{-13}
2	2.08	2.21	1.04	0.59	8×10^{-8}
3	2.58	2.63	0.86	0.53	1.62
4	2.64	2.68	0.66	0.41	1×10^{5}

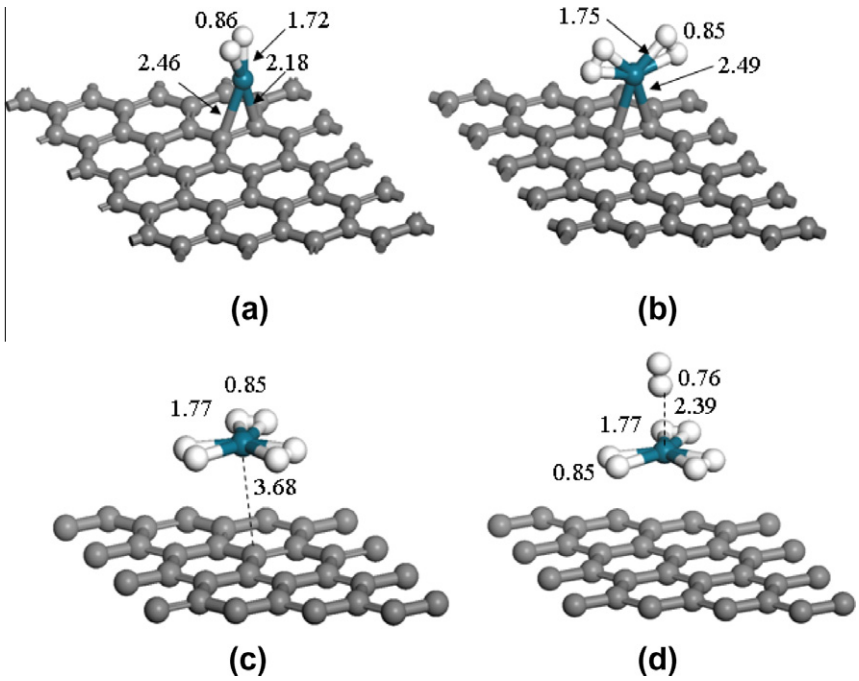

Fig. 5 – Geometry of $Pd(H_2)_n$ complexes on Pd-decorated graphene.

and

$$E_n^{PdC} = \frac{Pd(H_2)_n \text{ @ graphene} - Pd \text{ @ graphene} - nH_2}{n}$$

3.3. *Quantitative analysis of storage mechanisms and formation of Kubas-type complexes*

Adsorption isotherms for ACF and Pd-ACF measured at 25 °C are shown in Fig. 1. Pd-ACF exhibits a significantly larger hydrogen uptake capacity than ACF, despite comparable surface areas and porosity (Table 1). Four competing mechanisms should be considered to explain the data: (1) physisorption on carbon support, (2) hydride formation in large Pd particles, (3) H spillover and subsequent chemisorption to carbon or recombination to physisorbed H_2, and (4) multiple Kubas-type bonding to isolated Pd atoms. They are compared next.

(1) At higher pressure, physisorption on carbon support is dominant even at room temperature. Since Pd-ACF has practically the same surface area and porosity as Pd-free ACF (Table 1), it can be assumed that, at each pressure, physisorption on carbon in Pd-ACF is adequately represented by the hydrogen uptake on ACF. The uptake in excess of the amount adsorbed on support is the contribution of added Pd.

(2) *In situ* X-ray diffraction studies by Bhat et al. [48] demonstrated that hydrogen storage on Pd-ACF is accompanied by transformation of metallic Pd nanoparticles to Pd β-hydride. Assuming that the entire Pd content of Pd-ACF (i.e. 2.55 wt.%) was converted to β-$PdH_{0.67}$ upon exposure to hydrogen, the expected hydrogen uptake (on carbon support and in Pd hydride combined) should follow the dotted line in Fig. 1. However, adsorption measured at 20 bar is approximately 25–30% higher. This unaccounted difference may in reality be even larger based on reports that the H/Pd ratio in nanosized β-PdH_x particles may be lower than in the bulk ($x < 0.67$). Pd hydride nanoparticles, destabilized by multiple contacts with activated carbon may release H atoms easier than the bulk hydride [48] which may initiate H spillover.

(3) Hydrogen atoms spilled over to the support may bind strongly to unsaturated carbon atoms, as confirmed in this system by inelastic neutron spectroscopy [24]. Chemisorption to carbon is undesired because it may cause a small amount of hydrogen to be unavailable for desorption by simply lowering the pressure, as indeed observed from Fig. 1.

(4) Supported by identification of single Pd atoms, Kubas binding in Pd-ACF is a likely hypothesis which is being examined quantitatively next. Analysis of multiple

images recorded from numerous TEM samples revealed [40] that overall concentration of isolated Pd atoms within carbon matrix is roughly 0.05 atoms/nm^3. Considering the overall Pd concentration of 2.55 wt.% and the solid density of Pd-ACF (1.90 g/cm^3), we conclude that roughly 18 wt.% of total Pd present in the sample is in atomic form and can potentially form σ-bonded Kubas complexes with multiple H_2 per Pd atom.

The modeling results presented above indicate that single Pd atoms on flat graphene sheets may bind up to 4H_2 molecules per atom. However, the stability of Kubas complexes $Pd(H_2)_n$ @ graphene is expected to decrease with increase of n. Table 2 shows the binding energy, E_n^{PdC}, of each additional H_2 and the corresponding equilibrium hydrogen pressure for formation of each new adduct, p_n. The latter was calculated by applying the van't Hoff equation to the chemical equilibrium describing formation of $Pd(H_2)_n$ immobilized on graphene, Pd @ graphene + $nH_2 \rightleftarrows Pd(H_2)_n$ @ graphene:

$$n \ln p_n = -\ln K_n = \frac{\sum_{i=1}^{n} E_i^{PdC}}{k_B T} - \frac{n\Delta S}{R}$$

where K_n is the equilibrium constant for formation of $Pd(H_2)_n$, k_B is Boltzmann constant, R is the gas constant, $T = 300$ K, and ΔS is the change in entropy. Correct evaluation of the latter is critical for the accuracy of estimation. Following Durgun et al. [9] we used $\Delta S = -75.5$ J/mol K for the entropy change from H_2 gas at 1 bar to liquid form. This value is in the range of entropy changes estimated for H_2 adsorption on microporous carbon (66.5–76.5 J/mol K) [50]. As shown in Table 2, the first two H_2 molecules have high binding energies (0.96 and 0.59 eV) and correspondingly it is expected that exposure to very low pressure of H_2 would yield $Pd(H_2)_2$. The equilibrium pressure estimated for addition of the third H_2 molecule (binding energy 0.53 eV) is 1.6 bar, and therefore formation of $Pd(H_2)_3$ is expected in the experimental range of hydrogen measurements reported in Fig. 1. Addition of the fourth H_2requires pressure outside the experimental range.

Application of the GGA modeling results presented above to the Pd-ACF materials investigated in this study leads to the continuous red line in Fig. 1. It presents the expected hydrogen uptake from combined contributions of (1) physisorption to the carbon substrate; (2) 82 wt.% of total Pd in nanoparticles forming $PdH_{0.67}$; and (3) 18 wt.% of total Pd as isolated atoms forming Kubas complexes $Pd(H_2)_n$. The pressure dependence of n has been accounted for, based on data from Table 2. The plot overrates the experimentally observed H_2 uptake at low pressures, but underestimates it in the high pressure range. Given the obvious differences between the local environment of Pd atoms in the carbon matrix (Fig. 3) and the idealized graphene geometry used for modeling (Fig. 5), the agreement between GGA predictions and experiment is fairly good. The increasing slope of the isotherm in the high pressure regime may be an evidence that other processes, usually grouped under the umbrella name of spillover, may be active at high pressures (since the fourth H_2 molecule is not expected to bind within the pressure range of our measurements). A similar slope change (which continues to higher pressures) was reported for example by Li and Yang [51] in their study of H_2 adsorption on AX-21 and Pt-modified AX-21 carbons. They proposed a mechanism to explain pressure-dependent diffusivity of spilt-over hydrogen and the non-linear shape of isotherms. Such experimental isotherms (similar to that of Fig. 1) are frequently found for high surface area adsorbents containing not only Pd [16–24] but other metals as well [51–53]. However, the increase in slope of the continuous curve in Fig. 1 over a pressure range where binding of the third H_2 molecule to the ideal structures of Fig. 5 is complete while binding of the forth H_2 molecule is not expected may simply reflect the deviation of real material from the ideal flat structures assumed for modeling. Obviously, Pd atoms in the Pd-ACF matrix are structurally and energetically non-equivalent, as shown by the STEM images analyzed elsewhere [41]. In reality, graphenes are curved and wrinkled, with Pd atoms occupying positions on either the concave or convex side. This is expected to induce significant differences in the binding energy of Pd atoms to graphenes, with strong consequences on the binding energy of H_2 to Pd atoms [9,27]. If deviations from E_n^{PdC} values listed in Table 2 occur in the real Pd-ACF system, they would broaden the distribution of equilibrium formation pressure P of various $Pd(H_2)_n$ species. Last, occurrence of few atoms clusters, although not identified in our sample by electron microscopy, is not totally excluded. Calculations showed that interaction of molecular H_2 and small Pd clusters supported on carbon leads to dissociative adsorption of the first molecule, and migration of H atoms relative to the cluster [25,26,54,55]. Work continues in this direction and more results will be presented in a future publication.[1]

4. Conclusion

With the experimental means available to us today, we can provide only indirect arguments that Kubas-type complexes, $Pd(H_2)_n$ @ graphene, may occur in our system. Our intention is to project a new light on this additional mechanism that has not been discussed in sufficient details so far. We hope that our analysis and conclusion will incite further discussions which will elucidate the much debated mechanisms leading to enhanced hydrogen uptake in microporous adsorbents modified with TM catalysts.

We started from positive identification by high-resolution STEM of isolated Pd atoms dispersed and stabilized in the structure of activated carbon fibers, as reported in a separate letter. This is the experimental evidence that a necessary condition for the complexation mechanism to occur is met. We argue that the stabilization of single Pd atoms in Pd-ACF is the result of our particular synthesis procedure. For this synthesis, the $Pd(acac)_2$ precursor was mixed with the isotropic pitch precursor *prior* to all thermal treatment processes, which contributed to stabilization of a fraction of Pd as isolated atoms. Hydrogen adsorption measurements showed that Pd-modified ACF exhibit a 25–30% increase of hydrogen uptake at 25 °C and 20 bar, which cannot be

[1] Li S, Jena P. Pd-assisted hydrogen adsorption on graphene and carbon nanotubes, to be published (2010).

explained by formation of $PdH_{0.67}$ alone. First principle modeling showed that single Pd atoms on flat graphene structures are able to molecularly bind up to three H_2 molecules per Pd atom in the pressure range studied, forming Kubas-type complexes with H_2:Pd ratio larger than that of Pd hydride. Calculations of binding energies allowed us to estimate that the pressures corresponding to binding of first three H_2 molecules to Pd atoms are in the range of our experimental data. Based on these elements, we submitted that formation of Kubas-type complexes is a viable mechanism in our system, and we examined its relation with other accepted mechanisms (physisorption, hydride formation, spillover). We hypothesized that in favorable conditions Kubas-type binding occurs in parallel and overlapped with all other mechanisms accepted so far. Since quantitative analysis of STEM images determined that about 18% of all Pd is present in atomic form, we used this result to compare the contribution of Kubas complexes to the total H_2 uptake. The total adsorption calculated from combined H_2 physisorption to carbon support, hydride formation in Pd nanoparticles, and multiple binding of molecular H_2 to single Pd atoms was evaluated as a function of pressure. The agreement with measured adsorption data is fairly well, given the inherent differences between idealized model structures and the real system. Physisorption on carbon support dominates all other mechanisms, but in the high pressure range, a positive deviation of experimental data shows that these three mechanisms alone cannot fully explain the results. Since the separate contributions of physisorption and hydride formation are easily quantified, we propose that the complexation mechanism may explain some of the unaccounted excess uptake which so far was harbored under the umbrella name of spillover. The results and modeling suggest that spillover has increasing participation at high pressures, while complexation dominates at low and medium pressures. Therefore the contribution of spillover to the excess uptake in the initial pressure range might be smaller than previously thought for Pd-modified carbon where sample's history allowed stabilization of single transition metal atoms.

Acknowledgments

Research supported by the US Department of Energy, Basic Energy Sciences, Materials Sciences and Engineering Division (C.I.C., K.v.B., S.J.P., N.C.G.) and in part by the Scientific User Facilities Division, DOE Office of Basic Energy Sciences (K.v.B). K.v.B. and C.S.B. acknowledge additional financial support through UC Davis start-up funds (analysis of electron microscopy results). S.L. and P.J. (computational studies) acknowledge support from National Energy Research Scientific Computing Center (NERSC), which is supported by the Office of Science of US Department of Energy under Contract No. DE-AC02-05CH11231. Fruitful discussions with D.D. Edie and H. Tekinalp (Clemson University) and Mr. Tekinalp's contribution for synthesis of materials are gratefully acknowledged. Thanks are also due to Dr. Xianxian Wu for measurements of hydrogen adsorption data during a post-doctoral stage under ORNL Postdoctoral Associate Program administered jointly by ORISE and ORNL.

Appendix A. Supplementary data

Supplementary data associated with this article can be found, in the online version, at doi:10.1016/j.carbon.2011.05.021.

REFERENCES

[1] http://www.hydrogen.energy.gov/annual_review10_proceedings.html.
[2] Kubas GJ. Molecular hydrogen complexes: coordination of a σ bond to transition metals. Acc Chem Res 1988;21(3):120–8.
[3] Niu T, Rao BK, Jena P. Binding of hydrogen molecules by a transition–metal ion. Phys Rev Lett 1992;68(15):2277–80.
[4] Cabria I, Lopez MJ, Alonso JA. Enhancement of hydrogen physisorption on graphene and carbon nanotubes by Li doping. J Chem Phys 2005;123(20):204721–9.
[5] Yoon M, Yang S, Hicke C, Wang E, Geohegan D, Zhang Z. Calcium as the superior coating metal in functionalization of carbon fullerenes for high-capacity hydrogen storage. Phys Rev Lett 2008;100(20):206806-1–4.
[6] Lee H, Ihm J, Cohen ML, Louie SG. Calcium-decorated graphene-based nanostructures for hydrogen storage. Nano Lett 2010;10(3):793–8.
[7] Yildirim T, Ciraci S. Titanium-decorated carbon nanotubes as a potential high-capacity hydrogen storage medium. Phys Rev Lett 2005;94(17):175501–5.
[8] Yildirim T, Iniguez J, Ciraci S. Molecular and dissociative adsorption of multiple hydrogen molecules on transition metal decorated C_{60}. Phys Rev B 2005;72(15):153403–4.
[9] Durgun E, Ciraci S, Yildirim T. Functionalization of carbon-based nanostructures with light transition–metal atoms for hydrogen storage. Phys Rev B 2008;77(8):085405–85409.
[10] Phillips AB, Shivaram BS. High capacity hydrogen absorption in transition metal–ethylene complexes observed via nanogravimetry. Phys Rev Lett 2008;100(10):105505-1–4.
[11] Hamaed A, Trudeau M, Antonelli DM. H_2 storage materials (22 kJ/mol) using organometallic Ti fragments as σ-H_2 binding sites. J Am Chem Soc 2008;130(22):6992–9.
[12] Li S, Jena P. Comments on "Combinatorial search for optimal hydrogen-storage nanomaterials based on polymers". Phys Rev Lett 2006;97(20):209601-1.
[13] Sun Q, Wang Q, Jena P, Kawazoe Y. Clustering of Ti on a C_{60} surface and its effect on hydrogen storage. J Am Chem Soc 2005;127(42):14582–3.
[14] Krasnov PO, Ding F, Singh AB, Yakobson BI. Clustering of Sc on SWNT and reduction of hydrogen uptake: ab-initio all-electron calculations. J Phys Chem C 2007;111(49):17977–80.
[15] Pundt A, Kirchheim R. Hydrogen in metals: microstructural aspects. Ann Rev Mater Res 2006;36:555–608.
[16] Zlotea C, Cuevas F, Paul-Boncour V, Leroy E, Dibandjo P, Gadiou R, et al. Size-dependent hydrogen sorption in ultrasmall Pd clusters embedded in a mesoporous carbon template. J Am Chem Soc 2010;132(22):7720–9.
[17] Campesi R, Cuevas F, Leroy E, Hirscher M, Gadiou R, Vix-Guterl C, et al. In situ synthesis and hydrogen storage properties of PdNi alloy nanoparticles in an ordered mesoporous carbon template. Micropor Mesopor Mater 2009;117(1–2):511–4.
[18] Anson A, Lafuente E, Urriolabeitia E, Navarro R, Benito AM, Maser WK, et al. Hydrogen capacity of palladium-loaded carbon materials. J Phys Chem B 2006;110(13):6643–8.
[19] Back C, Sandi G, Prakash J, Hranisavljevic J. Hydrogen storage on palladium-doped sepiolite-derived carbon nanofibers. J Phys Chem B 2006;110(33):16225–31.
[20] Yoo E, Habe T, Nakamura J. Possibilities of atomic hydrogen storage by carbon nanotubes or graphite materials. Sci Technol Adv Mater 2005;6:615–9.

[21] Zacharia R, Kim KY, Fazle Kibria AKM, Nahm KS. Enhancement of hydrogen storage capacity of carbon nanotubes via spillover from vanadium and palladium nanoparticles. Chem Phys Lett 2005;412(4–6):369–75.
[22] Lupu D, Biris AR, Misan I, Jianu A, Holzhutter G, Burkel E. Hydrogen uptake by carbon nanofibers catalyzed by palladium. Int J Hydrogen Econ 2004;29(1):97–102.
[23] Gallego NC, Baker FS, Contescu CI, Wu X, Speakman SA, Tekinalp H, et al. Effect of Pd on the hydrogen adsorption capacity of activated carbon fibers. In: Carbon 2006, international conference on carbon, Aberdeen, Scotland, July 16–21, 2007.
[24] Contescu CI, Brown CM, Liu Y, Bhat VV, Gallego NC. Detection of hydrogen spillover in palladium-modified activated carbon fibers during hydrogen adsorption. J Phys Chem C 2009;113(14):5886–90.
[25] Singh AK, Ribas MA, Yakobson BI. H-spillover through the catalyst saturation: an ab-initio thermodynamics study. ACS Nano 2009;3(7):1657–62.
[26] Mushrif SH, Rey AD, Peslherbe GH. Energetics and dynamics of hydrogen adsorption, desorption and migration of a carbon-supported palladium cluster. J Mater Chem 2010;20(46):10503–10.
[27] Dag S, Ozturk Y, Ciraci S, Yildirim T. Adsorption and dissociation of hydrogen molecules on bare and functionalized carbon nanotubes. Phys Rev B 2005;72(15):155404-1–8.
[28] Gallego NC, Contescu CI, Bhat VV, van Benthem K, Tekinalp H, Edie DD. Palladium-doped nanoporous carbon fibers for hydrogen storage. In: Carbon 2008, international conference on carbon, Nagano, Japan, July 13–18; 2008.
[29] Wu X, Gallego NC, Contescu CI, Tekinalp H, Bhat VV, Baker FS, et al. The effect of processing conditions on microstructure of Pd-containing activated carbons fibers. Carbon 2008;46(1):54–61.
[30] Tekinalp HL, Cervo E, Thies MC, Contescu CI, Gallego NC, Edie DD. The effect of pitch composition on the adsorption behavior of Pd-doped ACF. In: Carbon 2007, international conference on carbon, Seattle, WA, USA, July 15–20; 2007. CD-ROM paper D051.
[31] Reimer L. Transmission electron microscopy. 2nd ed. Berlin, Heidelberg, New York: Springer; 1997.
[32] Varela M, Lupini AR, van Benthem K, Borisevich AY, Chisholm MF, Shibata N, et al. Materials characterization in the aberration-corrected scanning transmission electron microscope. Ann Rev Mater Res 2005;35:539–69.
[33] Kresse G, Furthmuller J. Efficient iterative schemes for *ab initio* total-energy calculations using a plane-wave basis set. Phys Rev B 1996;54(16):11169-86.
[34] Blöchl PE. Projector augmented-wave method. Phys Rev B 1994;50(24):17953–79.
[35] Wang Y, Perdew JP. Correlation hole of the spin-polarized electron gas, with exact small-wave-vector and high-density scaling. Phys Rev B 1991;44(24):13298–307.
[36] van Benthem K, Lupini AR, Kim M, Baik HS, Doh S, Lee JH, et al. Three-dimensional imaging of individual hafnium atoms inside a semiconductor device. Appl Phys Lett 2005;87(3):034104-1–3.
[37] van Benthem K, Lupini AR, Oxley MP, Findlay SD, Allen LJ, Pennycook SJ. Three-dimensional ADF imaging of individual atoms by through-focal series scanning transmission electron microscopy. Ultramicroscopy 2006;106(11–12):1062–8.
[38] Borisevich AY, Lupini AR, Pennycook SJ. Depth sectioning with the aberration-corrected scanning transmission electron microscope. Proc Natl Acad Sci USA 2006;103(9):3044–8.
[39] Wang SW, Borisevich AY, Rashkeev SN, Glazoff MV, Sohlberg K, Pennycook SJ, et al. Dopants adsorbed as single atoms prevent degradation of catalysts. Nat Mater 2004;3(3):143–6.
[40] Oh SH, van Benthem K, Molina SI, Borisevich AY, Luo WD, Werner P, et al. Point defect configurations of supersaturated Au atoms inside Si nanowires. Nano Lett 2008;8(4):1016–9.
[41] van Benthem K, Bonifacio CS, Contescu CI, Pennycook SJ, Gallego NC. STEM imaging of single Pd atoms in activated carbon fibers considered for hydrogen storage. Submitted as a letter to the editor of carbon (ms. CARBON-D-10-03099), in review; 2011.
[42] Basova YV, Edie DD. Precursor chemistry effects on particle size distribution in metal-containing pitch-based carbon fibers: a hypothesis. Carbon 2004;42(12–13):2748–51.
[43] Mushrif S, Rey AD, Peslherbe GH. Towards understanding palladium doping of carbon supports: a first-principles molecular dynamics investigation. J Mater Chem 2010;20:6859–62.
[44] Burgess WA, Pittman JJ, Marcus RK, Thies MC. Structural identification of the monomeric constituents if petroleum pitch. Energy Fuels 2010;24(8):4301–11.
[45] Borisevich AY, Lupini AR, Travaglini S, Pennycook SJ. Depth sectioning of aligned crystals with the aberration-corrected scanning transmission electron microscope. J Electron Microscopy 2006;55(1):7–12.
[46] O'Keefe MA, Allard LF, Blom DA. HRTEM imaging of atoms at sub-Ångstrom resolution. J Electron Microscopy 2005;54(3):169–80.
[47] van Benthem K, Peng YP, Pennycook SJ. Tomographic imaging of nanocrystals by aberration-corrected scanning transmission electron microscopy. Mater Res Soc Symp Proc 2005;839:3–7.
[48] Bhat VV, Contescu CI, Gallego NC. The role of destabilization of palladium hydride in the hydrogen uptake of Pd-containing activated carbons. Nanotechnology 2009;20(20):204011-1–10.
[49] Lopez-Corral I, German E, Volpe MA, Brizuela GP, Juan A. Tight-binding study of hydrogen adsorption on palladium decorated graphene and carbon nanotubes. Int J Hydrogen Energy 2010;35(6):2377–84.
[50] Bhatia SK, Myers AL. Optimum conditions for adsorptive storage. Langmuir 2006;22(4):1688–700.
[51] Li Y, Yang RT. Hydrogen storage on platinum nanoparticles doped on superactivated carbon. J Phys Chem C 2007;111(29):11086–94.
[52] Wang L, Yang RT. New sorbents for hydrogen storage by spillover – a review. Energy Environ Sci 2008;1(2):268–79.
[53] Wang L, Yang RT. Hydrogen storage properties of carbons doped with ruthenium, platinum, and nickel nanoparticles. J Phys Chem C 2008;112(32):12486–94.
[54] Moc J, Musaev DG, Morokuma K. Adsorption of multiple H_2 molecules on Pd_3 and Pd_4 clusters: a density functional study. J Phys Chem A 2000;104(49):11606–14.
[55] Fayet P, Kaldor A, Cox DM. Palladium clusters: H_2, D_2, N_2, CH_4, CD_4, C_2H_4, and C_2H_6 reactivity and D_2 saturation studies. J Chem Phys 1990;92(1):254–61.